Acta Geotechnica
DOI 10.1007/s11440-015-0419-3

CrossMark

RESEARCH PAPER

Unidirectional cyclic resistance of Ticino and Toyoura sands from centrifuge cone penetration tests

Vincenzo Fioravante[1] · Daniela Giretti[1]

Received: 27 February 2015 / Accepted: 6 October 2015

Abstract The evaluation of the undrained cyclic resistance of sandy deposits is required to forecast the soil behaviour during an earthquake (liquefaction, cyclic mobility); due to the difficulties in obtaining undisturbed samples of most liquefiable soils, it is usually deduced from field test results such as cone penetration tests. This paper proposes a methodology to evaluate the undrained cyclic resistance from normalised cone resistance of two well-studied silica sands (Ticino and Toyoura), with different mineralogy, one mainly composed of feldspar, the other of quartz. The determination of the cyclic resistance of Ticino and Toyoura sands was achieved through undrained cyclic triaxial tests on reconstituted specimens. The tip resistance was deduced from CPTs performed in centrifuge with a miniaturised piezocone on homogeneous reconstituted models. Both the undrained cyclic and tip resistances were correlated with the state parameter ψ. Results of centrifuge and triaxial tests were combined through ψ to deduce the cyclic resistance ratio CRR directly from the normalised cone resistance. The shape of the curve relating CRR to the normalised cone resistance resulted unusual respect to all the recognised curves widespread in the geotechnical literature. The aim of the proposed correlations is to provide a useful instrument to improve the actual knowledge on liquefaction and to give a contribution based on the critical state soil mechanics framework to the development of refined correlations between the cyclic resistance of a sand and the results of cone penetration tests.

✉ Vincenzo Fioravante
vincenzo.fioravante@unife.it

[1] University of Ferrara, Ferrara, Italy

Keywords Centrifuge tests · Cone penetration tests · Cyclic resistance · Cyclic triaxial tests · Liquefaction · Sand · State parameter

1 Introduction

Cyclic liquefaction is a phenomenon during which granular uncemented saturated soils (gravel, sand and low plasticity silt) lose much of their strength and stiffness for a short interval of time, but long enough to cause significant failures.

After the severe 1964 earthquake of Niigata in Japan, during which widespread liquefaction phenomena took place causing deaths and extensive financial losses, many researchers worldwide started research programmes aimed at defining methods of analysis and prediction of liquefaction susceptibility of soils.

The occurrence of liquefaction depends on the cyclic shear loading induced by an earthquake and on the cyclic resistance of the soil; the latter, due to the difficulties in obtaining undisturbed samples of most liquefiable soils, is usually deduced from field test results interpreted via empirical correlations which provide the link between cyclic resistance and various test indices. The collection of a great number of field test data and observations of real occurrences, allowed developing empirical approaches expressed as graphs, where the in situ test index is plotted versus the cyclic stress resistance. A bounding line defines two areas: one where liquefaction is possible and the other where liquefaction is not expected. Initially the methods were based on the results of standard penetration tests [37]; then, as the SPT was progressively replaced by cone penetration test (more repeatable and reliable), CPT-based methods of liquefaction assessment have become the most used in practice engineering [15, 26, 29, 32, 41].

Journal : Large 11440 | Dispatch : 29-10-2015 | Pages : 16
Article No. : 419 | ☐ LE | ☐ TYPESET
MS Code : AGEO-D-15-00067 | ☑ CP | ☑ DISK

In general, the cone penetration resistance q_c and the undrained cyclic resistance ratio, CRR of an uncemented and unaged soil depend on the material properties (i.e. mineralogy, shape, asperities and roughness of grains, grading and fabric) and the state of the soil (stress level and density). The latter two quantities can be expressed by the state parameter ψ (i.e. the distance along the void ratio axis of a given state from the critical state line, [4]), which is an indicator of the direction of volumetric strains, $\delta\varepsilon_v$, (dilation or contraction) during shearing. This means that q_c and CRR are governed by the volumetric behaviour of the soil:

- The stress ratio necessary to reach liquefaction at a defined number of cycles increases as ψ decreases, since at a given depth the denser is the soil, the lower is its tendency to develop positive excess pore water pressure when sheared in undrained conditions.
- The penetration resistance of a soil, at a given depth, is governed by the effective stress increment around the tip: the amount of the volumetric strains governs the stress change respect to the geostatic level of stress.

Therefore the direction and the amount of the volumetric strains can be expressed by the state parameter ψ [i.e. $\delta\varepsilon_v = f(\psi)$], ~~the latter~~ which can be used to link directly CRR to the tip resistance of CPTs.

In ~~these~~ this paper this link is weaved using the results of centrifuge CPT tests and cyclic undrained triaxial tests carried out using two well-known Italian and Japanese sands: Ticino (TS4) and Toyoura (TOS). All the centrifuge tests (on TS4 and TOS) and the triaxial tests on TS4 belong to the database of ISMGEO (Istituto Sperimentale Modelli Geotecnici, formerly ISMES, Seriate—BG—Italy) and were carried out mainly in the '90. The cyclic behaviour of TOS was derived from published data quoted below.

The results of cone penetration tests performed in centrifuge, using a miniaturised piezocone, confirmed and strengthened what observed in previous studies based on large calibration chamber (CC) tests, that is the existence of a simple exponential relationship between a normalised cone resistance and the state parameter ψ [5, 22].

The cyclic triaxial test results were interpreted to define a correlation between the state parameter and the cyclic resistance ratio, CRR at a given number of cycles N, for the two studied sands.

Finally results of centrifuge and triaxial tests were combined to infer the cyclic resistance ratio directly from the normalised cone resistance. The correlation proposed, which applies to clean, uncemented, normally consolidated, young sands, resulted with an unusual shape respect to all the recognised curves widespread in the geotechnical literature: a possible physical explanation ~~has been~~ is provided.

2 The testing soils

The soils investigated in this research are two well-known Italian and Japanese silica sands, Ticino and Toyoura sands, hereafter referred to as TS4 and TOS, respectively.

TS4 was used to carry out both centrifuge cone penetration tests and static and cyclic triaxial (Tx) tests. TOS was used for the centrifuge CPTs, while its static and cyclic mechanical behaviour was derived from previous publications [25, 38–40].

The soils used for laboratory and centrifuge tests have the grain size distribution and the index properties given in Fig. 1 and Table 1. TS4 is a uniform coarse to medium sand made of angular to subrounded particles and composed of 30 % quartz, 65 % feldspar and 5 % mica [1, 2, 21]; TOS is a uniform fine sand consisting of subrounded to subangular particles and composed of 90 % quartz, 8 % feldspar and 2 % mica [21].

2.1 Monotonic behaviour of TS4 and TOS

The mechanical behaviour of TS4 was investigated through a series of monotonic and cyclic Tx tests selected from a large database of tests performed at the ISMGEO laboratory. The details of the tests, whose results have not been published before, are given in Tables 2 and 3. All the tests were carried out on sample reconstituted by pluvial deposition in air of the dry sand, subsequently saturated in the

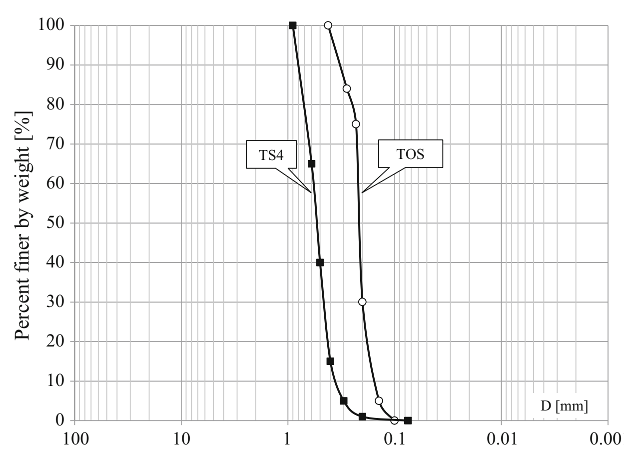

Fig. 1 Grain size distribution of Ticino and Toyoura sands

Journal : Large 11440 | Dispatch : 29-10-2015 | Pages : 16
Article No. : 419 | LE | TYPESET
MS Code : AGEO-D-15-00067 | CP | DISK

Table 1 Index properties of Toyoura and Ticino sand

Sand	γ_{min} kN/m^3	γ_{max} kN/m^3	e_{min} –	e_{max} –	G_s –	D_{50} mm	U_c –
TOS ([21] and this experimentation)	13.09	16.13	0.612	0.986	2.65	0.22	1.31
TOS [40]	13.15	16.28	0.597	0.977	2.65	0.17	1.7
TOS [38]	13.15	16.20	0.605	0.977	2.64	0.175	1.52
TS4 ([1, 2, 21] and this experimentation)	13.64	16.67	0.574	0.923	2.68	0.53	1.3

triaxial cell with CO_2 circulation, flushing of deaerated water and adequate back pressure.

The monotonic tests consisted in Tx compression on both isotropic and anisotropic consolidated samples. The applied consolidation mean effective stress p'_c ranged from 50 to 870 kPa. The samples where both normally consolidated and over consolidated, the overconsolidation ratio ranging from 1 to 8. The failure was reached applying standard drained and undrained compression stress paths ($\Delta\sigma_a > 0$ and $\Delta\sigma_r = 0$), except in one test during which the mean effective stress was kept constant ($\Delta p' = 0$; $\Delta\sigma_a = -2\Delta\sigma_r$). For comparison, a series of Tx drained and undrained tests carried out by Golder Associates ([22], www.golder.com/liq) as part of an internal project was also considered in the definition of the mechanical properties of TS4.

The states of the samples at critical states are plotted in Fig. 2; they were fitted with a power law (according to Li and Wang [24]) as follows:

$$e_{cs} = \Gamma - \lambda \cdot (p'/p_a)^{\alpha} \tag{1}$$

where: $p' = (\sigma'_a + 2\sigma'_r)/3$, mean effective stress; σ'_a and σ'_r = axial and radial effective stress; $p'_a = 101$kPa atmospheric pressure; Γ, λ, α = material constants determining the critical state line position and shape, whose values were ~~have been~~ obtained from data best fitting, i.e. $\Gamma = 0.923$; $\lambda = 0.046$, $\alpha = 0.5$.

The stress ratio at critical state M_c (triaxial compression) resulted equal to 1.36, which corresponds to a critical state angle $\varphi'_{cv} = 34°$. This is illustrated in Fig. 3a, b: Fig. 3a shows the critical state conditions of all the tested samples in the q–p' plane (where $q = \sigma'_a - \sigma'_r$ is the stress deviator in axial symmetry conditions), interpolated with a linear regression, whose slope is $M_c = 1.36$; Fig. 3b shows the maximum values of the stress ratio $\eta = q/p'$ measured during drained tests as a function of the corresponding minimum value of the dilatancy D, defined as:

$$D = \delta\varepsilon_v / \delta\varepsilon_q \tag{2}$$

$\delta\varepsilon_v$ = volumetric strain increment; $\delta\varepsilon_q$ = deviatoric strain increment. The $\eta_{max} - D_{min}$ conditions can be interpolated by a linear regression, whose intercept at zero dilatancy is $M_c = 1.36$.

The mechanical behaviour of TOS has been widely investigated by several authors [12, 20, 38–40]. The TOS critical state line (CSL) in the e–p' plane assumed in the present work was defined on the base of a large series of drained and undrained triaxial compression tests on specimen reconstituted at different initial states using the wet tamping method, as reported by Verdugo, Verdugo and Ishihara [39, 40]. The index properties of the tested sand are given in Table 1. The material constants determining the critical state line position and shape (Eq. 1) were calibrated by Li and Dafalias [25] and resulted: $\Gamma = 0.934$, $\lambda = 0.019$, $\alpha = 0.7$.

The CSL so defined is plotted in Fig. 2 and compared with that of TS4. As to the stress ratio at critical state M_c, it resulted equal to 1.25, which corresponds to a critical state angle $\varphi'_{cv} = 31°$.

2.2 Cyclic behaviour of TS4 and TOS

The undrained cyclic Tx tests on TS4 were performed on reconstituted samples (as for the monotonic tests, the reconstitution was carried out by pluvial deposition in air of the dry sand and subsequent saturation), isotropically normally consolidated at a mean effective stress $p'_c = 100$kPa. Only to one samples was applied an isotropic pressure of 200 kPa. A direct consequence of testing at same p'_c is that making reference to the density of specimens is equivalent to making reference to the average state parameter, ψ_{avg}, defined, according to Been and Jefferies [4], as:

$$\psi = e - e_{cs} \tag{3}$$

where e = current void ratio; e_{cs} = void ratio on the CSL at the same p'.

The tested specimens were reconstituted at three values of void ratio: medium void ratio ($e_{avg} = 0.742$, which, with reference to Eqs. 1, 3, corresponds to $\psi_{avg} = -0.132$), low void ratio ($e_{avg} = 0.676$, $\psi_{avg} = -0.201$) and very low void ratio ($e_{avg} = 0.582$, $\psi_{avg} = -0.295$).

The states of all the samples laid below the CSL, i.e. at the end of the consolidation all the specimens had $\psi < 0$. Fig ~~Figure~~ 4a–d shows the results of the test TS4_13_8 in terms of axial deformation ε_a versus the number of cycles N (Fig. 4a); deviatoric stress q versus ε_a (Fig. 4b); excess

Journal : Large 11440 Dispatch : 29-10-2015 Pages : 16
Article No. : 419 ☐ LE ☐ TYPESET
MS Code : AGEO-D-15-00067 ☑ CP ☑ DISK

Table 2 Monotonic compression triaxial tests on Ticino Sand

Test	Type of consolidation	Stress path	End of consolidation						Critical state			
			e_c –	σ'_{ac} kPa	σ'_{rc} kPa	p'_c kPa	q'_c kPa	OCR –	e_{cs} –	p'_{cs} kPa	q_{cs} kPa	η_{cs} –
Monotonic drained tests												
TS4-171	CK	$\sigma'_r = \text{const}$	0.759	500.3	235.2	323.5	265.1	1.2	0.810	438.5	610.0	1.39
TS4-172	CK	$\sigma'_r = \text{const}$	0.773	400.5	220.6	280.6	179.9	1.5	0.824	397.3	530.0	1.33
TS4-CK5	CK	$\sigma'_r = \text{const}$	0.790	877.1	370.0	539.0	507.1	1	0.809	677.0	921.0	1.36
TS4-K6	CK	$\sigma'_r = \text{const}$	0.730	1446.7	581.0	869.6	865.7	1	0.770	1061.0	1440.0	1.36
TS4-K8	CK	$\sigma'_r = \text{const}$	0.798	773.5	341.0	485.2	432.5	1	0.827	620.0	837.0	1.35
TS4-M32	CI	$\sigma'_r = \text{const}$	0.640	800.0	800.0	800.0	0.0	1	0.678	1543.3	2230.0	1.44
TS4-R14	CK	$p'_r = \text{const}$	0.698	1199.8	506.6	737.7	693.1	1	0.778	726.2	980.0	1.35
TS4-U21	CI	$\sigma'_r = \text{const}$	0.756	301.5	298.0	299.2	3.5	4	0.814	524.7	680.0	1.30
TS4-U22	CI	$\sigma'_r = \text{const}$	0.796	124.9	124.0	124.3	0.9	4	0.856	212.3	265.0	1.25
TS4-U24	CI	$\sigma'_r = \text{const}$	0.760	125.0	118.0	120.3	7.0	4	0.827	204.7	260.0	1.27
TS4-U36	CK	$\sigma'_r = \text{const}$	0.751	200.0	246.0	230.7	−46.0	6	0.785	419.8	521.4	1.24
TS4-U38	CK	$\sigma'_r = \text{const}$	0.760	50.3	59.0	56.1	−8.7	6	0.852	102.3	130.0	1.27
TS4-U50	CK	$\sigma'_r = \text{const}$	0.785	74.8	94.0	87.6	−19.2	8	0.847	164.0	210.0	1.28
TS4-V9	CK	$\sigma'_r = \text{const}$	0.687	1154.5	437.0	676.2	717.5	1	0.761	810.0	1119.0	1.38
TS4-C262*	CI	$\sigma'_r = \text{const}$	0.851	200.0	200.0	200.0	0.0	1	0.819	323.7	374.0	1.16
TS4-C263*	CI	$\sigma'_r = \text{const}$	0.781	200.0	200.0	200.0	0.0	1	0.796	336.7	406.8	1.21
Monotonic undrained tests												
1101*	CI	$\sigma'_r = \text{const}$	0.867	307.8	307.8	307.8	0.0	1	0.867	146.9	154.9	1.05
TS4-1103*	CI	$\sigma'_r = \text{const}$	0.888	302.0	302.0	302.0	0.0	1	0.877	94.7	102.5	1.08
TS4-1105*	CI	$\sigma'_r = \text{const}$	0.898	279.2	279.2	279.2	0.0	1	0.898	36.0	37.8	1.05
TS4-1106*	CI	$\sigma'_r = \text{const}$	0.85	503.7	503.7	503.7	0.0	1	0.850	277.9	334.1	1.20
TS4-H0	CI	$\sigma'_r = \text{const}$	0.810	799.8	799.7	799.7	0.0	1	0.810	845.0	1125.9	1.33
TS4-H1	CI	$\sigma'_r = \text{const}$	0.831	400.1	399.8	399.9	0.2	1	0.831	486.3	649.3	1.34
TS4-H2	CI	$\sigma'_r = \text{const}$	0.827	499.6	499.6	499.6	0.0	1	0.827	582.1	787.7	1.35
TS4-H3	CI	$\sigma'_r = \text{const}$	0.826	600.1	599.8	599.9	0.3	1	0.826	686.9	921.4	1.34
TS4-H4	CI	$\sigma'_r = \text{const}$	0.812	700.0	700.2	700.1	−0.1	1	0.812	727.8	983.1	1.35
TS4-H5	CI	$\sigma'_r = \text{const}$	0.808	799.9	800.0	799.9	−0.1	1	0.808	750.7	1022.2	1.36
TS4-H6	CK	$\sigma'_r = \text{const}$	0.816	750.3	340.9	477.4	409.5	1	0.816	780.6	1079.3	1.38
TS4-H7	CK	$\sigma'_r = \text{const}$	0.844	750.4	366.7	494.6	383.7	1	0.844	571.5	764.2	1.34
TS4-H8	CK	$\sigma'_r = \text{const}$	0.846	750.2	359.6	489.8	390.6	1	0.846	560.8	753.5	1.34
TS4-H10	CK	$\sigma'_r = \text{const}$	0.839	600.5	285.5	390.5	314.9	1	0.839	529.9	703.0	1.33
TS4-H11	CK	$\sigma'_r = \text{const}$	0.842	750.2	344.1	479.4	406.1	1	0.842	527.2	699.3	1.33
TS4-H12	CK	$\sigma'_r = \text{const}$	0.841	900.3	427.8	585.3	472.5	1	0.841	640.9	849.1	1.32
TS4-H13	CK	$\sigma'_r = \text{const}$	0.825	1050.1	478.5	669.0	571.6	1	0.825	682.2	911.0	1.34
TS4-H14	CK	$\sigma'_r = \text{const}$	0.826	1199.5	555.8	770.4	643.8	1	0.826	716.5	962.3	1.34
TS4-H15	CK	$\sigma'_r = \text{const}$	0.812	750.1	357.7	488.5	392.4	1	0.812	692.3	943.7	1.36
TS4-H16	CK	$\sigma'_r = \text{const}$	0.813	750.0	359.2	489.5	390.9	1	0.813	638.6	868.2	1.36

CK, anisotropic consolidation; CI, isotropic consolidation

OCR over consolidation ratio

* data from Golder (samples reconstituted by wet tamping) [22]; www.golder.com/liq

pore pressure Δu versus N (Fig. 4c); q versus mean effective stress p' (Fig. 4d, where the critical state lines in compression and extension ~~have been~~ are also reported as dashed lines). The sample ~~has been~~ was subjected to a stress deviator $\Delta q = \Delta\sigma_a = \pm\, 62$ kPa (i.e. to a cyclic stress ratio $\mathrm{CSR}^{\mathrm{TX}} = \Delta\sigma_a / 2p'_c = 0.31$).

Journal : Large 11440 Dispatch : 29-10-2015 Pages : 16
Article No. : 419 LE TYPESET
MS Code : AGEO-D-15-00067 CP DISK

Table 3 Cyclic undrained triaxial tests on Ticino Sand

Test	Type of consolidation	End of consolidation				Failure		
		e_c	q_c^*	OCR	ψ	CSR^{TXa}	N^a	R_u^a
		–	kPa	–	–	–	–	–
TS4_13_1	CI	0.740	0	1	−0.137	0.21	6	0.95
TS4_13_4	CI	0.730	0	1	−0.147	0.17	25	0.96
TS4_13_6	CI	0.700	0	1	−0.177	0.18	149	0.95
TS4_13_7	CI	0.700	0	1	−0.177	0.33	4.5	0.87
TS4_13_8	CI	0.640	0	1	−0.237	0.31	14.5	0.91
TS4_13_9	CI	0.640	0	1	−0.237	0.24	19	0.97
TS4_13_11	CI	0.760	0	1	−0.099	0.29	1.5	0.8
TS4_13_13	CI	0.760	0	1	−0.117	0.26	3	0.9
TS4_13_14	CI	0.730	0	1	−0.147	0.175	14	0.87
TS4_13_15	CI	0.730	0	1	−0.147	0.16	617	0.92
TS4_13_17	CI	0.700	0	1	−0.177	0.32	7	0.95
TS4_13_23	CI	0.707	0	1	−0.171	0.23	9	0.96
TS4_14_1	CI	0.586	0	1	−0.291	0.41^b	60^b	0.95
TS4_14_2	CI	0.58	0	1	−0.297	0.28	220	0.97
TS4_14_3	CI	0.581	0	1	−0.297	0.13^b	900^b	0.95
TS4_14_4	CI	0.58	0	1	−0.297	0.38	140^b	0.95

~~*OCR* over consolidation ratio~~ delete

delete apex

$R_u = \Delta u / p'_c$

[a] values at $\varepsilon_a^{DA} = 5\,\%$

[b] The failure criteria $\varepsilon_a^{DA} = 5\,\%$ was not met; in the table the number of cycles when $R_u = 0.95$ are reported

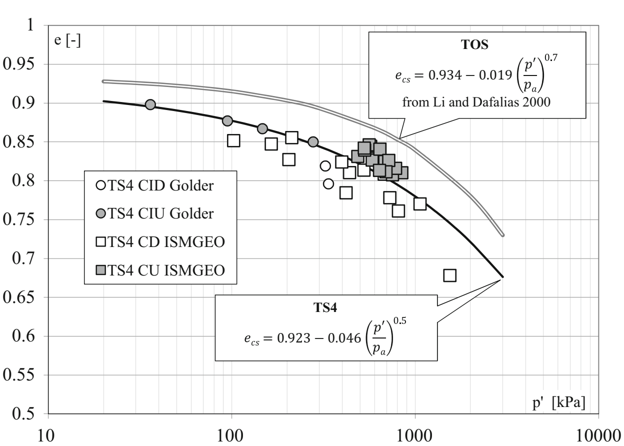

Fig. 2 Critical state lines of Ticino and Toyoura (from [25]) sands

During the test, the specimen underwent a typical response known as “cyclic mobility”. Axial strains and pore pressure built up gradually during each cycle and the effective stress p' reduced. Since application of the first load cycle, the specimen exhibited an alternating incrementally dilative response (p' increasing) and incrementally contractive response (p' decreasing). The failure condition, assumed in this study as the condition at which $\varepsilon_a^{DA} = 5\,\%$, was reached between the 14th and 15th cycle and it is evidenced with an empty dot in the Figures (being ε_a^{DA} the cyclic double amplitude, DA, axial strain). At this point $\Delta u \approx 90$ kPa and the pore pressure ratio was $R_u = \Delta u / p'_c \approx 0.9$; R$_u$ remained almost constant at larger N. When the test was approaching the failure condition, the stress path started going back and forth, with an excursion almost confined between the two critical state lines in extension and compression. It is worth noting that no monotonic triaxial test was carried out in extension loading conditions; assuming that φ'_{cv} does not depend on the Lode’s angle θ, the stress ratio at critical state applicable to extension loading path, M_e was assumed equal to −0.94 and plotted in Fig. 4d.

The stress–strain curves were initially elliptical loops; when the sample was approaching the failure condition, the hysteresis loops assumed a typical S inverted shape. When the stress path approached the hydrostatic condition, the soil stiffness and resistance dropped towards zero; as the applied deviatoric load increased, the specimen exhibited strain hardening and regained stiffness and resistance.

All the failure conditions of the tested samples are given in Table 3 and are represented in Fig. 5a, in terms of applied cyclic stress ratio and number of cycles at $\varepsilon_a^{DA} = 5\,\%$. In the Figure, the cyclic stress ratio for triaxial

Journal : Large 11440 Dispatch : 29-10-2015 Pages : 16
Article No. : 419 LE TYPESET
MS Code : AGEO-D-15-00067 CP DISK

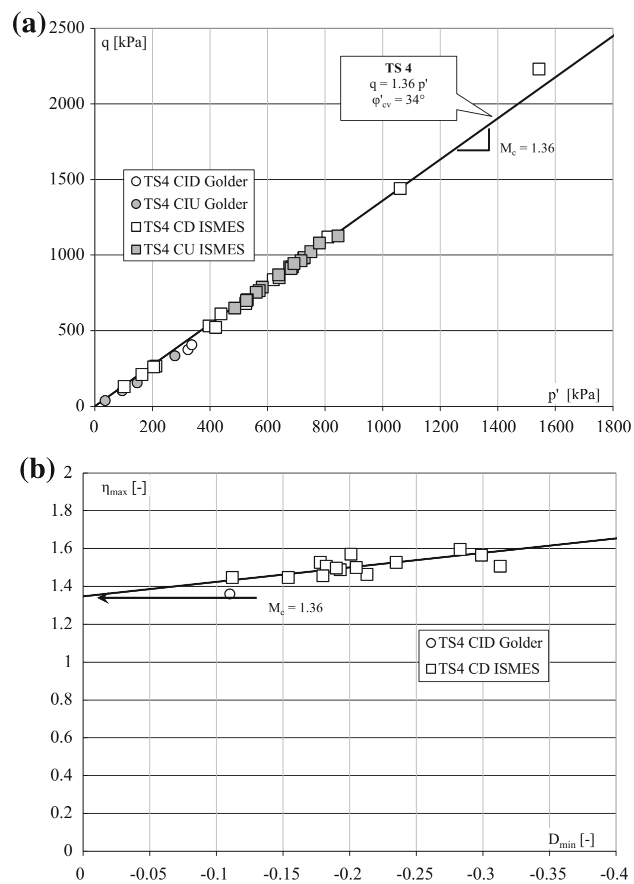

Fig. 3 Ticino Sand: **a** critical states in the q–p' plane; **b** relation between peak strain and minimum dilatancy

condition ~~has been~~ was corrected into cyclic stress ratio for simple shear conditions (CSR^{SS}) via equation [17, 18]:

$$CSR^{SS} = CSR^{TX}(1 + 2k_0)/3 \tag{4}$$

where: $k_0 = \sigma'_r/\sigma'_a$ = stress ratio at rest, computed as a function of the critical state shear resistance angle φ'_{cv} for normally consolidated samples using the equation of [19]. For TS4, $k_0 = 0.44$ and $CSR^{SS} = 0.63 \times CSR^{TX}$.

In Fig. 5a the cyclic resistance of medium void ratio samples ($\psi_{avg} = -0.132$) is represented by empty circles, that of dense sample ($\psi_{avg} = -0.201$) by full squares, that of very dense samples ($\psi_{avg} = -0.295$) by grey triangles. It is worth noting that in all the tests, the R_u values at failure (computed from the maximum value of Δu measured during the loading cycle at which ε_a^{DA} equalled 5 %) ranged from 0.8 to 0.97. Only two samples (TS4_14_01 and TS4_14_03) did not match the failure criteria and the axial strain at the end of the tests was $\varepsilon_a^{DA} < 5\,\%$. For these samples the condition $R_u = 0.95$, reached at $N = 60$ and $N = 900$, respectively, was assumed as the failure condition.

As to the cyclic behaviour of TOS referred to in the present paper, it was investigated through a cooperative laboratory testing programme, undertaken by five laboratories in Japan, which included 81 undrained cyclic triaxial tests on medium void ratio ($e_{avg} = 0.778$ at the end of consolidation, $\psi_{avg} = -0.17$) and low void ratio ($e_{avg} = 0.684$, $\psi_{avg} = -0.231$) TOS samples, isotropically compressed at an initial effective mean stress of $p'_c = 98$ kPa. All the samples were reconstituted by pluvial deposition in air of the dry sand and were normally consolidated in triaxial cell. The index properties of the tested sand are summarised in Table 1. The results were reported by Toki et al. [38] in terms of cyclic stress ratio for triaxial conditions CSR^{TX} and number of cycles N, at four values of ε_a^{DA}.

In Fig. 5b are reported the values of CSR^{SS} at $\varepsilon_a^{DA} = 5\,\%$ and the related number of cycles; in the Figure, the cyclic resistance of samples with an average state parameter, $\psi_{avg} = -0.231$, is represented by full squares, that of samples with $\psi_{avg} = -0.127$, by empty circles. The cyclic stress ratio for simple shear conditions CSR^{SS} was computed from the applied CSR^{TX} via Eq. 4, i.e. $CSR^{SS} = 0.66 \times CSR^{TX}$, being $k_0 = 0.485$.

Fig. ~~Figure~~ 5a, b ~~show~~ shows that the two tested sands have similar behavioural trends. Groups of samples relating to a given ψ_{avg} describe clear relationships between CSR^{SS} and N, whose slope in the semi-log plane is strongly dependent on ψ.

These relationships were interpreted with a power function of N which accounts for the dependence of the cyclic resistance on ψ as follows:

$$CSR^{SS} = \frac{a(1-\psi)^b}{N^{c(1-\psi)}} \tag{5}$$

where $a = 0.071$, $b = 7.8$, $c = 0.177$, TS4 empirical constants determined by fitting 17 data; $a = 0.037$, $b = 10.7$, $c = 0.247$, TOS empirical constants determined by fitting 66 data.

In Fig. 5a, b are reported sets of curves computed using Eq. 5. For each group of tests (characterised by a given ψ_{avg}), the curves ~~have been~~ were computed for the minimum and maximum value of ψ of the group. A good agreement between the test results and the equation~~s~~ can be recognised, as shown also in Fig. 6, where the cyclic stress ratios computed via Eq. 5 are plotted versus the applied CSR^{SS}: an error of ±20 % was considered acceptable.

Equation 5 allows the estimation of the cyclic resistance ratio CRR^{SS} for any number of equivalent cycles, e.g. for $N = 15$:

Journal : Large 11440 | Dispatch : 29-10-2015 | Pages : 16
Article No. : 419 | LE | TYPESET
MS Code : AGEO-D-15-00067 | CP | DISK

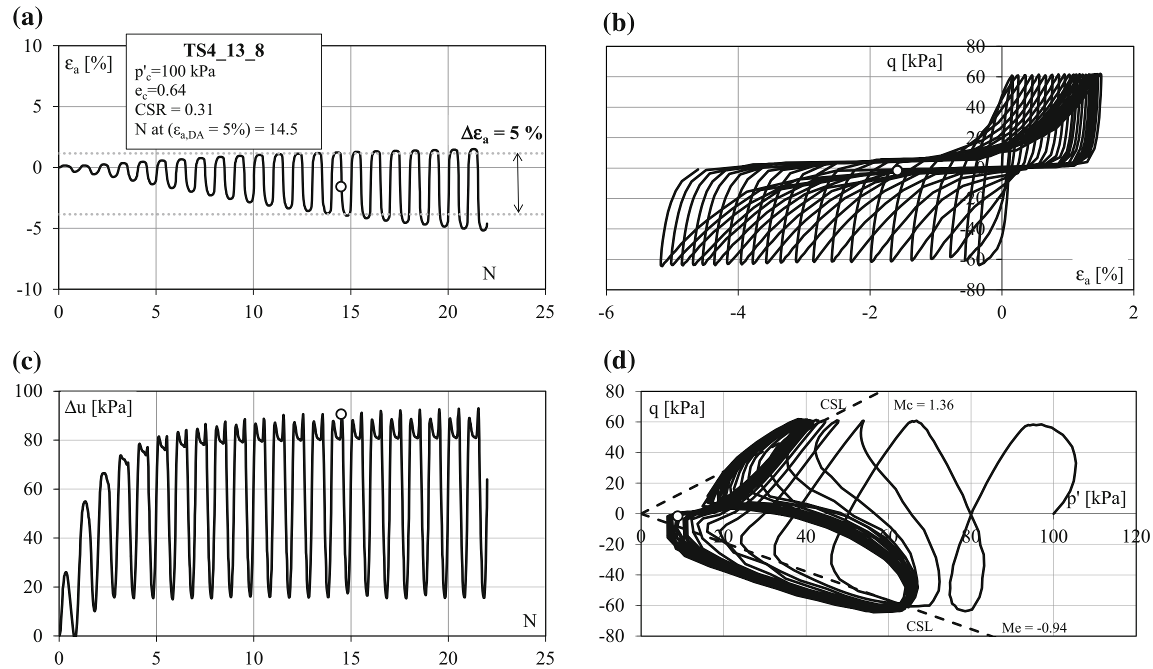

Fig. 4 Cyclic triaxial test TS4_13_8 on Ticino Sand: **a** axial strain ε_a versus number of cycles N; **b** stress deviator q versus ε_a; **c** excess pore pressure Δu versus N; **d** q versus mean effective stress p'

$$\mathrm{CRR}^{\mathrm{SS}}_{15,\mathrm{TS4}} = 0.071 \cdot (1-\psi)^{7.8} / 15^{0.177(1-\psi)} \tag{6a}$$

$$\mathrm{CRR}^{\mathrm{SS}}_{15,\mathrm{TOS}} = 0.037 \cdot (1-\psi)^{10.7} / 15^{0.247(1-\psi)} \tag{6b}$$

The computed $\mathrm{CRR}^{\mathrm{SS}}_{15}-\psi$ ~~correlation~~ correlations for TS4 and TOS ~~is~~ are shown in Fig. 7. $\mathrm{CRR}^{\mathrm{SS}}_{15}$ decreases as ψ increases and tends to zero for positive ψ values.

The cyclic resistance of TS4 is higher than that of TOS at the same value of the state parameter ψ. The following considerations can explain this difference:

- All the samples were isotropically consolidated at an effective mean stress of about 100 kPa, so there is no static bias due to different initial stress conditions.
- The effect of soil fabric [13, 23, 27] as consequence of sample preparation procedure can be considered of minor influence, since, while recognising the unavoidable differences in the internal procedures adopted by different laboratories, both the TS4 and TOS samples were reconstituted by pluviating the dry sand in air.
- TS4 has a higher critical stress ratio M_c than TOS since its grains are more irregular and angular, so the friction work among particles is greater in TS4 than TOS: in cyclic loading more energy is dissipated in TS4 respect to TOS and the undrained resistance is greater [33].
- TS4 and TOS have different mineralogy: TOS is richer in quartz minerals, which are stiffer and stronger than feldspar minerals, of which is mainly composed TS4. In general TS4 is more compressible than TOS, as can be deduced by the slope of their CSL in the e–p' plane (see Fig. 2). Higher compressibility may imply that a larger part of the undrained cyclic load applied during tests on TS4 samples is spent to compress and rearrange the sand grains than in TOS.

3 Centrifuge tests

3.1 The ISMGEO seismic geotechnical centrifuge

The model cone penetration tests were performed using the ISMGEO seismic geotechnical centrifuge (ISGC), which is a beam centrifuge made up of a symmetrical rotating arm with a diameter of 6 m, a height of 2 m and a width of 1 m, which gives it a nominal radius of 2 m. The arm holds two swinging platforms, one used to carry the model container and the other the counterweight. During the tests, the platforms lock horizontally to the arm to prevent transmitting the working loads to the basket suspensions. An outer fairing covers the arm; arm and fairing concurrently rotate to reduce air resistance and perturbation during flight. The centrifuge has the potential of reaching an acceleration of 600g at a payload of 400 kg. The maximum dimensions of the model are length = 1 m, height = 0.8 m, with = 0.5 m; further details can be found in [3].

Journal : Large 11440 Dispatch : 29-10-2015 Pages : 16
Article No. : 419 LE TYPESET
MS Code : AGEO-D-15-00067 CP DISK

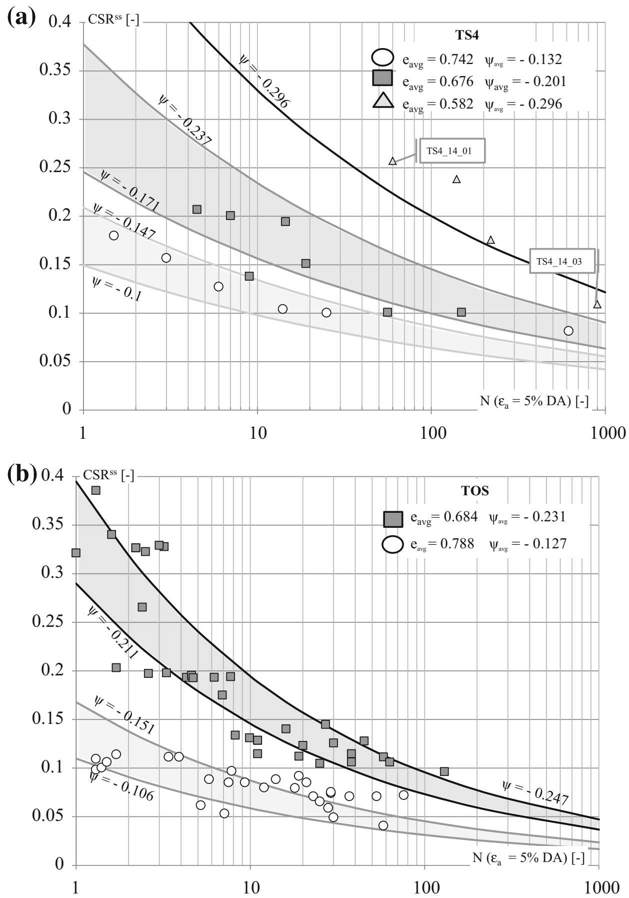

Fig. 5 Cyclic strength of **a** Ticino and **b** Toyoura sands in unidirectional simple shear conditions (data of TOS from Toki et al. [38])

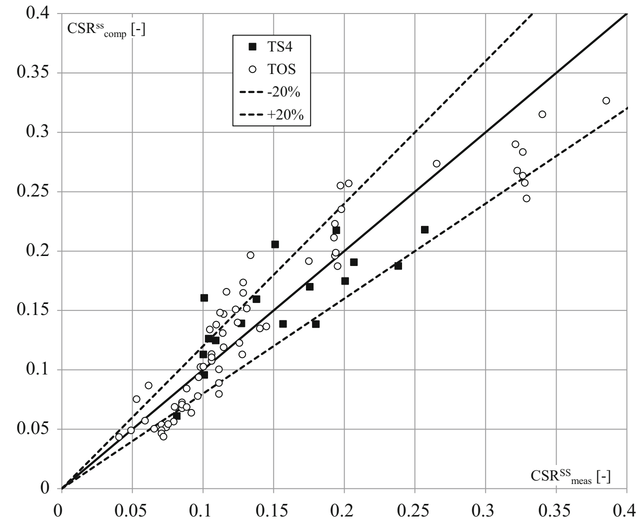

Fig. 6 Computed versus measured CSR^{SS} for TS4 and TOS

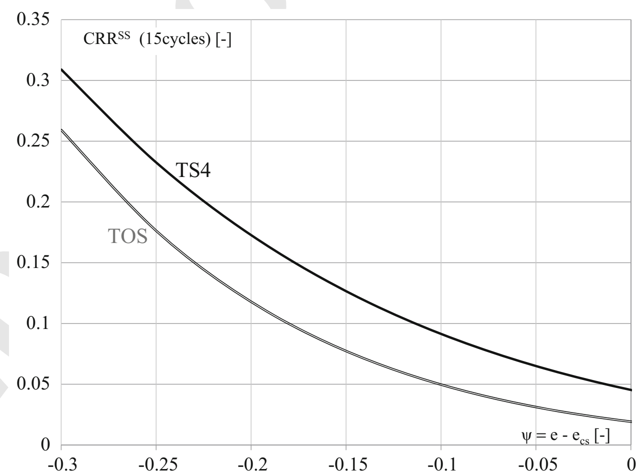

Fig. 7 Cyclic resistance ratio at 15 cycles for unidirectional simple shear conditions (CRR^{SS}_{15}) as a function of state parameter ψ for TS4 and TOS

In centrifuge modelling, a model geometrically scaled down N times and prepared from the prototype material is accelerated N times the earth gravity: the centrifuge acceleration reproduces the same stress and strain fields in the model as in the prototype. With this technique, self-weight stresses and gravity dependent processes are correctly reproduced and the observations from the model can be related to the prototype using the similarity relationships.

Respect to CPTs carried out in the large ISMGEO Calibration Chamber (soil specimen diameter = 1.2 m, height = 1.5 m), those performed in centrifuge have the advantage of giving a whole q_c profile over a wide range of stresses and ψ values, rather than a single q_c value associated with the specific values of the state parameter and the applied stress level of a single sample, but have the disadvantage of one fixed boundary conditions (rigid walls) and scale effects which were minimised as described below.

3.2 Test programme and procedures

The test programme consisted of 37 centrifuge CPTs, 27 carried out on dry TS4 models, 10 on dry TOS models, as detailed in Tables 4 and 5. The tests were carried out at three levels of centrifugal acceleration: 30*g*–50*g*–80*g* (where g is the earth gravity), and the models were characterised by three levels of void ratio: low, medium and high void ratio. It should be noted that [6] compared

Journal : Large 11440 | Dispatch : 29-10-2015 | Pages : 16
Article No. : 419 | ☐ LE | ☐ TYPESET
MS Code : AGEO-D-15-00067 | ☑ CP | ☑ DISK

Table 4 Main properties of Ticino Sand models

Test	Acceleration a (g)	Unit weight[a] γ_{dry} (kN/m^3)	Void ratio[a] e_c (–)	Relative density[a] D_R (%)	Model height H_m (cm)	Prototype height H_p (m)
TS4-1	30	14.30	0.834	25	34.7	10.40
TS4-2	30	14.40	0.822	28	34.6	10.37
TS4-3	80	14.45	0.815	30	34.5	27.58
TS4-4	80	14.53	0.805	34	34.5	27.57
TS4-5	30	16.11	0.629	84	35.4	10.61
TS4-6	30	15.94	0.646	79	35.1	10.52
TS4-7	80	16.02	0.638	82	34.8	27.84
TS4-8	80	16.03	0.637	82	34.9	27.90
TS4-11	30	14.54	0.804	34	43.9	13.17
TS4-12	30	14.31	0.834	26	43.9	13.18
TS4-13	80	14.44	0.816	31	43.8	35.07
TS4-14	80	14.47	0.813	32	43.9	35.14
TS4-15	80	15.09	0.738	53	44.3	35.41
TS4-16	30	15.18	0.728	56	44.4	13.31
TS4-17	50	15.22	0.724	57	44.3	22.16
TS4-18	50	15.24	0.721	58	44.3	22.15
TS4-19	30	16.19	0.620	87	44.5	13.35
TS4-20	80	16.27	0.613	89	44.5	35.58
TS4-21	50	16.21	0.619	87	44.5	22.23
TS4-22	50	16.16	0.623	86	44.5	22.23
TS4-23	50	14.42	0.819	30	44.0	22.01
TS4-24	50	14.47	0.813	32	44.0	22.02
TS4-25	30	14.41	0.821	29	44.0	13.21
TS4-26	80	14.41	0.821	29	44.0	35.24
TS4-28	50	16.23	0.617	88	44.4	22.22
TS4-29	50	15.25	0.720	58	44.3	22.15
TS4-30	30	14.38	0.824	28	44.0	13.20

[a] Values at the end of the in-flight consolidation (assumed constant with depth)

the results of CC CPT tests carried out on a certain number of dry and saturated samples of Ticino sand, characterised by the same test conditions, showing a little influence of the saturation on the measured penetration resistance. Similar conclusions were reached by [35] comparing CC tests performed on dry and nearly saturated sample of quartz Ottawa sand.

The tests were carried out using the ISMGEO miniaturised electrical piezocone, which has a diameter $d_c = 11.3$ mm, an apex angle of 60°, a sleeve friction 11.3 mm in diameter and 37 mm long. One load cell measures the cone resistance and another one measures the cone resistance plus the shaft friction, up to forces of 9.8 kN. A Druck PDCR42 pressure transducer (35 bar capacity) is installed on the tip for interstitial pressure measurements in saturated models.

Each soil model was reconstituted at 1g to the target void ratio by pluviating in air the dry sand into a cylindrical container using a travelling sand spreader. It should be noted that the same reconstitution procedure was adopted for centrifuge as for triaxial samples. The target density was obtained by calibrating the height of fall and the size of the spreader hole. The cylindrical container had an internal diameter of $D = 400$ mm, a height of 630 mm and rigid walls to avoid lateral displacements of the soil. The model container internal diameter was large enough to minimise rigid wall boundary effects, according to Bolton et al. [7]: container size effect, $D/d_c = 35.4 > 30$; side boundary effect, $s/d_c = 17.2 > 10$, where $s = 194.35$ mm is the distance of the cone shaft from the side wall. The models height ranged from 345 to 445 mm.

After the deposition, a very rigid frame, which held the piezocone, two linear displacement transducers (LDT) to monitor the cone displacement and the sand surface settlement, respectively, and a hydraulic actuator, was fixed to the container walls. ~~Figure~~ Fig. 8 shows a model scheme and a model picture with a view of the surface settlement transducer and the miniaturised piezocone, before the penetration.

Journal : Large 11440 | Dispatch : 29-10-2015 | Pages : 16
Article No. : 419 | LE | TYPESET
MS Code : AGEO-D-15-00067 | CP | DISK

Table 5 Main properties of Toyoura Sand models

Test	Acceleration a (g)	Unit weight[a] γ_{dry}(kN/m^3)	Void ratio[a] e_c (–)	Relative density[a] D_R (%)	Model height H_m (cm)	Prototype height H_p (m)
TYC1	30	15.71	0.655	88	34.8	10.45
TYC2	30	15.71	0.654	89	34.9	10.47
TYC3	80	15.69	0.657	88	34.9	27.90
TYC4	80	15.75	0.650	90	34.8	27.84
TYC5	80	14.66	0.774	57	34.9	27.91
TYC6	80	14.58	0.783	54	34.8	27.82
TYC7	80	15.08	0.724	70	34.8	27.81
TYC8	80	15.02	0.730	68	35.0	28.01
TYC9	30	15.12	0.719	71	34.8	10.43
TYC10	30	15.04	0.728	69	34.8	10.44

[a] Values at the end of the in-flight consolidation (assumed constant with depth)

Each model was then loaded in the centrifuge and accelerated to the target acceleration. As it was subjected to the acceleration field in the centrifuge, the soil surface slightly settled due to the self-weight and the model compressed, as monitored by the LDT. When the surface settlements ended up, the cone penetration test was carried out applying a penetration rate of 2 mm/s. The test penetration was interrupted at 20 d_c of distance from the container bottom to avoid rigid boundary effects [7]. Only one test per model was performed in the central axis of each sample accelerated at one target value.

The unit weight γ_{dry}, void ratio e and relative density D_R values reported in Tables 4 and 5 refer to the end of in-flight compression and were assumed constant with depth in test interpretation. In first approximation, the variation of the void ratio due to the increase in stresses with depth was neglected since its effect on the test results was considered a minor effect. The soil models at the end of the in-flight compression can be considered as normally consolidated. It is worth noting that the states of all the soil models at the end of the consolidation lied below the reference critical state lines.

3.3 Test results

To measure a q_c profile over a wide range of stresses, three (TS4) or two (TOS) acceleration levels were imposed by the centrifuge to soil models of the same dimensions, each reproducing different stress intervals: the acceleration of 30 g reproduced a mean effective stress interval from about 30 to 100 kPa; 50g reproduced a stress range from about 50 to 200 kPa; 80g reproduced a stress interval from about 100 to 300 kPa. In order to take into account the progressive mobilisation of the cone resistance from the model free surface [36], the measures registered in the first 10 d_c of penetration from the surface were removed. The results of centrifuge CPTs are shown in Fig. 9a, b, where the measured tip resistance q_c is plotted as a function of the mean effective stress p' for TS4 and TOS, respectively. The reported q_c measures are not affected by top and bottom boundary effects. In the Figures the "operative" stress intervals reproduced by the acceleration levels are evidenced.

The black lines in the Figures represent q_c measured in the models with the lower void ratio ($e \approx 0.63$ and $e \approx 0.65$ for TS4 and TOS, respectively); the dark grey curves refer to the models with the intermediate void ratio ($e \approx 0.73$, TS4 and $e \approx 0.72$, TOS); the light grey curves represent the models with the higher void ratio ($e \approx 0.82$, TS4 and $e \approx 0.78$, TOS).

It should be noted that during the centrifuge tests the actual horizontal stresses, σ'_h cannot be measured. The mean effective stress p' of the soil at rest was evaluated as:

$$p' = \sigma'_v(1 + 2k_0)/3 \tag{7}$$

where σ'_v = vertical effective stress, computed accounting for the acceleration field distortion; $k_0 = 0.44$ for TS4 and $k_0 = 0.485$ for TOS (computed using the equation of [19]).

The test results show that the soil models were rather homogeneous and the tests were repeatable so that the q_c values measured on models with similar void ratio subjected to different accelerations almost described a unique cone resistance profile. The unavoidable scatter can be attributed to slight differences in void ratio among models.

As expected, the penetration resistance strongly depended on the void ratio. For a given value of e, a behavioural trend, comparable to that observed in large calibration chamber tests in homogeneous sand models can be observed, i.e. a less than linear increase in q_c with the stress level.

Journal : Large 11440 | Dispatch : 29-10-2015 | Pages : 16
Article No. : 419 | □ LE | □ TYPESET
MS Code : AGEO-D-15-00067 | ✔ CP | ✔ DISK

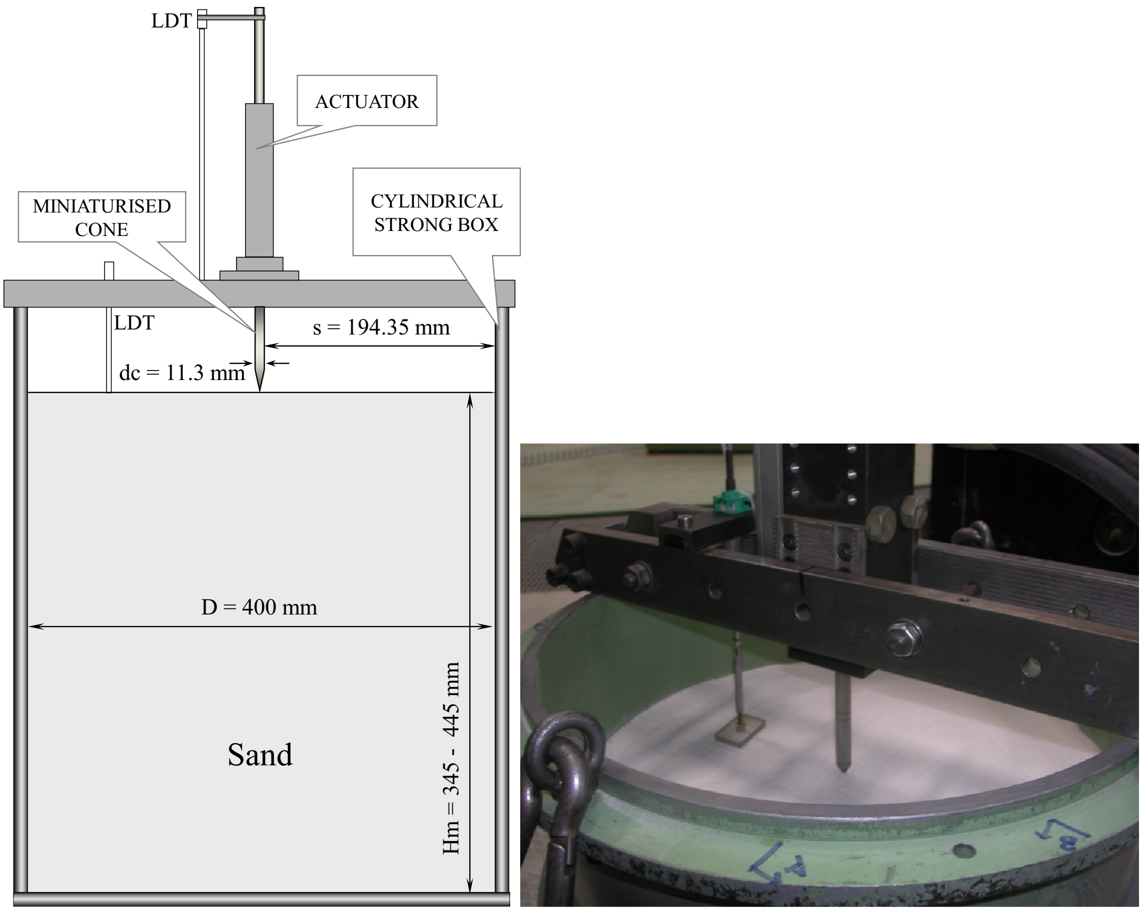

Fig. 8 Model scheme and model picture with a view of the ISMGEO miniaturised piezocone before penetration

This behaviour was originally interpreted considering the cone resistance as a square root function of the vertical stress [2]. In recent years there have been several publications regarding the appropriate stress normalisation of q_c [8, 11, 21, 26, 28, 31, 32, 42]. Idriss and Boulanger [14] suggested that the stress exponent should vary with relative density, where the exponent is close to 1.0 in loose sands and less than 0.5 in dense sands. Been et al. [5] analysing the results of calibration chamber tests on Monterey sand at constant state parameter, showed that the cone resistance is directly proportional to stress level.

insert "the"

3.4 Test interpretation

To better understand the physical meaning of the nonlinear increase in q_c with the stress level, the other variables which influence the cone penetration resistance have to be considered and, if possible, analysed separately.

As shown by [9, 10, 34, 22], the zone around the penetrometer is characterised by intense shearing with substantial changes in void ratio, which can decrease (contraction) or, more likely, increase (dilation). This tendency to dilate causes a stress increase around the tip (herein simply called $\delta p'$), respect to the stress value at rest. $\delta p'$ is proportional to the dilatancy D, which in turn can be linked to the value of the state parameter ψ at rest, before penetration [22].

As a working hypothesis, q_c ~~has been~~ was considered affected by two major contributions:

- the first given by the overburden stresses acting at the depth of the tip, herein represented by the mean effective stress p';
- the second, and more relevant at depths commonly investigated via CPTs (<50 m), due to the increment of stresses around the tip, $\delta p'$, caused by the volumetric change induced by the penetration, $\delta\varepsilon_v$, that can be represented by ψ, as the second independent variable.

In functional form, it can be written:

$$q_c = f[p', \delta p'(\psi)];\ [\mathrm{FL}^{-2}] \tag{8a}$$

or, in non-dimensional form:

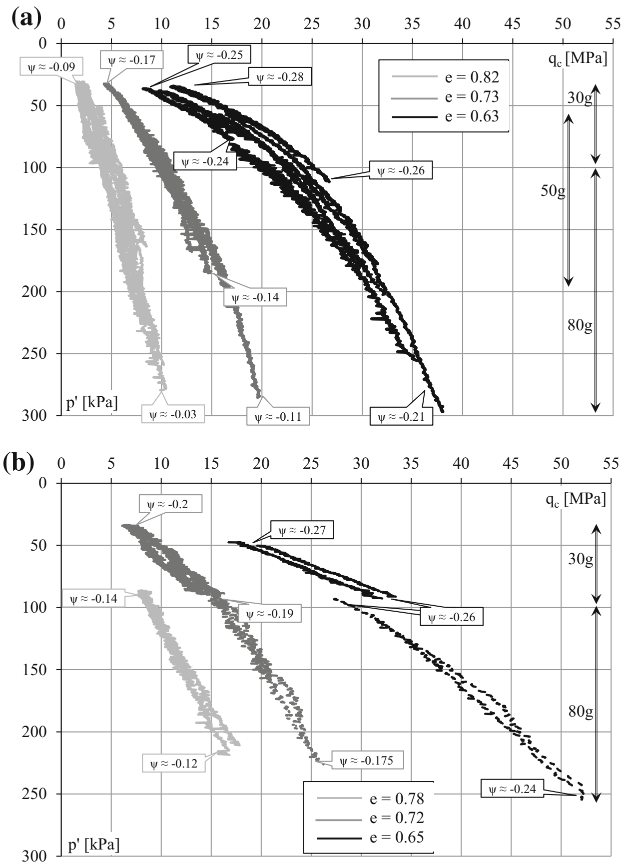

Fig. 9 CPTs in **a** TS4 and **b** TOS: tip resistance q_c as a function of mean effective stress p' (computed adopting $k_0 = 0.44$ for TS4 and $k_0 = 0.485$ for TOS)

$$\frac{q_c}{p_a} = f\left(\frac{p'}{p_a}, \frac{\delta p'(\psi)}{p_a}\right) \tag{8b}$$

In a homogeneous soil model with constant void ratio with depth (after the achievement of in-flight equilibrium and before test penetration), ψ at rest increases as the depth increases, so the tendency of a soil to dilate reduces with depth. This is shown in Fig. 10a, where the e–p' profiles at rest of the TS4 soil models, at the depths progressively crossed by the penetrometer, are plotted; each soil model is represented by a horizontal segment (the variation of e with depth was assumed negligible in the test interpretation). In the Figure is shown the critical state line of TS4 and, for each ~~test~~ model, are evidenced two e–p' points relating to the first and last depths relevant for the penetration test. The ψ values relating to these two points were computed from the CSL. They are reported in Fig. 9a, b, to evidence that the cone penetrated ~~a~~ progressively less dilative ~~soil~~ models due to the rise in ψ.

From each CPT, values of q_c, related to some values of ψ at rest, were selected: each e–p' profile of the soil models was intersected in Fig. 10a (for TS4 only) with constant $-\psi$ curves (called iso—ψ). The q_c values, measured at depths relating to the intersections, were picked out, normalised by the reference atmospheric pressure ($p_a = 101$ kPa) and plotted in Fig. 10b.

The function which better interpolates the normalised cone resistance at constant ψ, is a power law:

$$q_c/p_a = f(p'/p_a)^{\beta} \tag{9}$$

The same procedure was followed for the CPTs carried out on TOS models (for sake of briefness not reported here). Based on the best fit of all the analysed constant ψ cone resistance profiles, β resulted equal to 0.8 and it expresses the contribution on q_c of the overburden stresses acting at the depth of the tip. This value, slightly lower than the unitary exponent suggested by [22] for interpreting constant ψ cone resistance profiles, was adopted in this paper and the measured cone resistance was normalised as follows:

$$f(p'/p_a)^{\beta} = (q_c/p_a) \cdot (p_a/p')^{0.8} = q_c^* \tag{10}$$

and plotted as a function of p' in Fig. 11a, b, for TS4 and TOS, respectively. The values of ψ at rest at the initial and final points of the q_c^* profiles are also indicated. Since the effect of p' on q_c ~~has been~~ was almost removed through the normalisation, the Figures evidence the effect of ψ on the cone resistance: as the cone crosses less dilative soil (rising of ψ with depth), q_c^* reduces nonlinearly due to the reduction in $\delta p'$ around the tip. Had ψ been constant in each model, we would have obtained almost constant q_c^* profiles with depth.

To evaluate the effect of ψ on the normalised tip resistance, the q_c^* values obtained from CPTs on both TS4 and TOS models, were plotted versus ψ, as reported in Fig. 12. In the Figure, the black continuous lines represent TS4 CPTs, the grey lines TOS CPTs. The following considerations can be made:

- irrespective of the different intrinsic properties of the two sands, once that the overburden stress effect on q_c was almost removed through the normalisation of q_c, the $q_c^* - \psi$ curves of TS4 and TOS have a very similar trend and are very close each other;
- the individual trend of each sand can be interpreted with the following equation (adapted from [5]):

$$q_c^* = k \cdot e^{-m\psi} \tag{11}$$

where m and k are dimensionless fitting parameter, equal to:

Journal : Large 11440 | Dispatch : 29-10-2015 | Pages : 16
Article No. : 419 | ☐ LE | ☐ TYPESET
MS Code : AGEO-D-15-00067 | ☑ CP | ☑ DISK

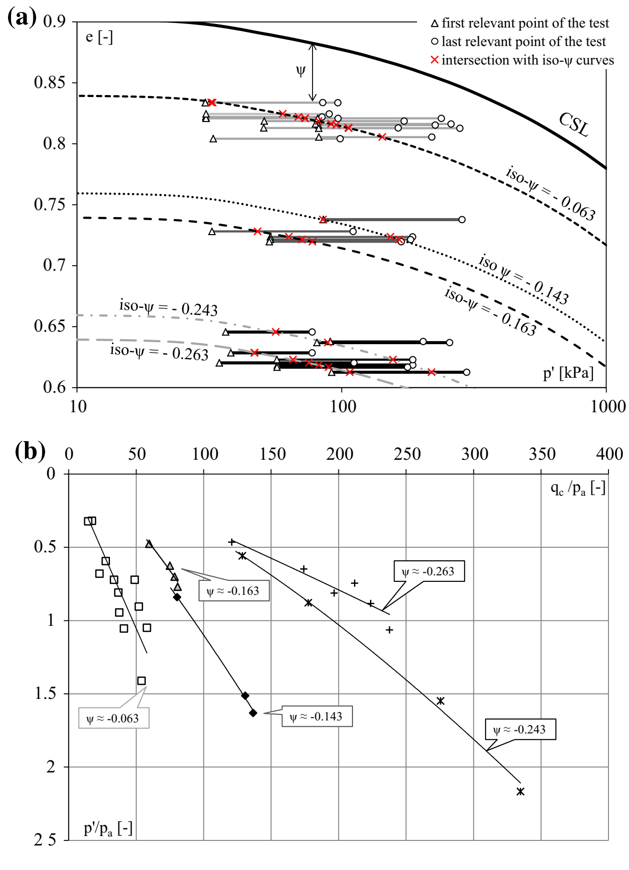

Fig. 10 CPTs in TS4: **a** e–p' relationships, **b** cone resistance at constant values of the state parameter ψ

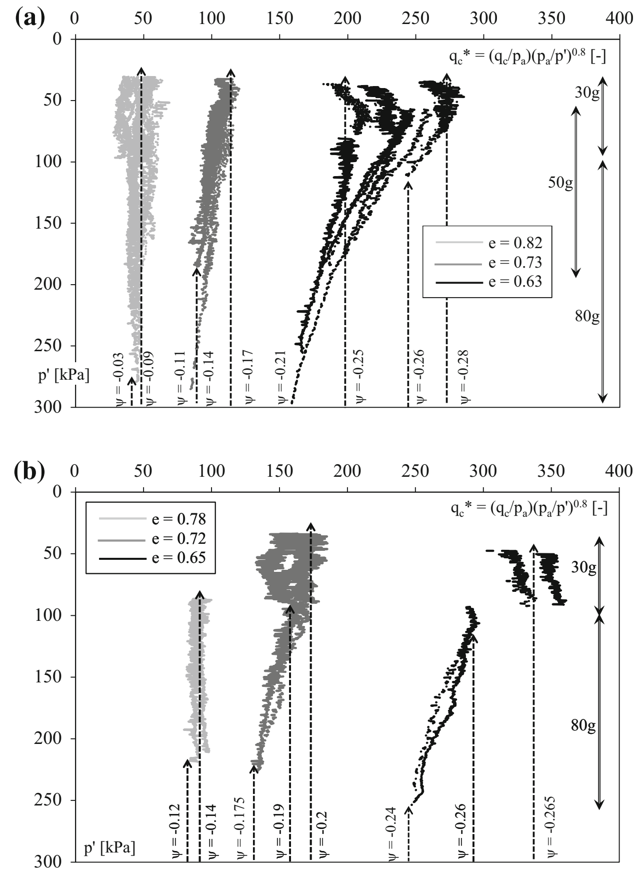

Fig. 11 Normalised tip resistance q_c^* as a function of mean effective stress p': **a** TS4, **b** TOS

- $m = 8.1$, $k = 28.3$ for TS4 (12720 data, $R^2 = 0.96$);
- $m = 9.8$, $k = 23.9$ for TOS (3808 data, $R^2 = 0.97$).

The TS4 and TOS interpolation curves are plotted in Fig. 12, as black and grey double lines, respectively.

Physically, the intercept k represents the q_c^* value when $\psi = 0$, while m allows to establish the contribution of dilatancy on the cone penetration resistance at a given value of ψ.

Equation 11 expresses the effect of dilation (or $\delta p'$) on the normalised cone resistance. Together with Eq. 10, it allows to re-write Eq. 8b as follows:

$$(q_c/p_a) = (p'/p_a)^{\beta} k \cdot e^{-m\psi} \quad (12)$$

in which the first term of the product to the right of the equal sign represents the functional dependency of q_c on the overburden stresses acting at the depth of the point; the second, the dependency of the cone resistance on the soil tendency to dilate.

From Fig. 12 it results that $(q_c^*)_{TOS} > (q_c^*)_{TS4}$, particularly at $\psi < -0.15$. This difference can be attributed to the lower crushability that subrounded quartz grains of dense TOS exhibit during penetration respect to subangular mainly feldspar grains of dense TS4.

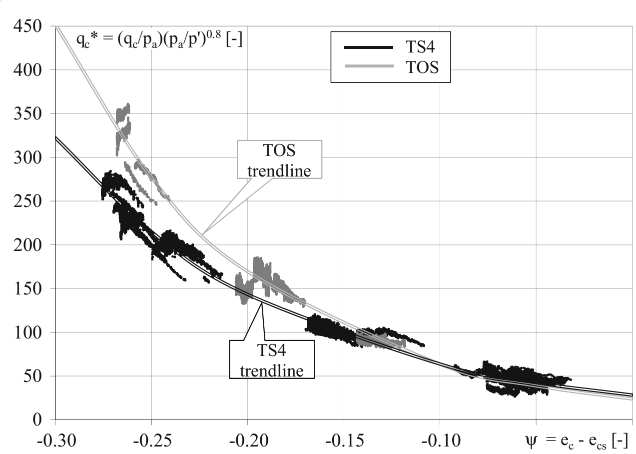

Fig. 12 Normalised q_c^* versus the state parameter for TS4 and TOS

Journal : Large 11440 Dispatch : 29-10-2015 Pages : 16
Article No. : 419 LE TYPESET
MS Code : AGEO-D-15-00067 CP DISK

4 CRR from CPT through ψ

To evaluate CRR directly from q_c, the state parameter ψ was assumed as independent variable which governs both the cyclic stress resistance and the normalised cone resistance of the tested soils.

Equations 5 and 11 were combined into Eq. 13 to obtain a direct correlation between q_c^* and the cyclic resistance ratio at N cycles for simple shear condition, CRR_N^{SS}:

$$\mathrm{CSR}_N^{SS} = \frac{a\left[1+\frac{1}{m}\ln\left(\frac{q_c^*}{k}\right)\right]^b}{N^{c\left[1+\frac{1}{m}\ln\left(\frac{q_c^*}{k}\right)\right]}} \tag{13}$$

For $N = 15$ cycles, Eq. 13 can be re-written as:

$$\mathrm{CRR}_{15}^{SS} = \frac{a\left[1+\frac{1}{m}\ln\left(\frac{q_c^*}{k}\right)\right]^b}{15^{c\left[1+\frac{1}{m}\ln\left(\frac{q_c^*}{k}\right)\right]}} \tag{14}$$

where a, b, c, m and k are the fitting parameters of Eqs. 5 and 11.

The $\mathrm{CRR}_{15}^{SS}-q_c^*$ relationships obtained for the two tested sands are plotted in Fig. 13; the upper black curve is relating to TS4, the lower grey to TOS.

These curves have different concavity respect to the bounding lines which separates cases of liquefaction and no-liquefaction in the “traditional” assessment charts [14, 29, 30, 41] based on superficial evidences for a number of case histories.

Apart from the downward concavity, which may require to be confirmed by further experimentation, the major difference between the traditional bounding lines and those presented in this paper is that the former imply almost an infinite cyclic resistance for a normalised cone resistance larger than a given value, while the relationship here proposed shows a more progressive mobilisation of the cyclic resistance, as the normalised cone resistance increases.

The downward concavity resulted from the computations carried out: a given change of the state parameter produces a change of the normalised tip resistance δq_c^* greater than the variation of the cyclic resistance, δ(CRR). From the trend lines of Figs. 7 and 12, the increments of q_c^* and CRR were computed with respect to their values at $\psi = 0$, as follows:

$$\delta q_c^* = \left(q^*_{c,\psi} - q^*_{c,\psi=0}\right)/q^*_{c,\psi=0} \tag{15}$$

$$\delta\mathrm{CRR} = \left(\mathrm{CRR}_{\psi} - \mathrm{CRR}_{\psi=0}\right)/\mathrm{CRR}_{\psi=0} \tag{16}$$

and plotted versus ψ in Fig. 14. The Figure shows that to achieve a given increment of CRR a larger increment of q_c^* is required (i.e. downward concavity).

The trend shown in Fig. 13 has to be confirmed by more experimental data, and the new correlation proposed will require a calibration on a wider number of sands to be usable in the engineering practice.

It is worth noting that the obtained relationships were derived under specific test conditions:

- the soil samples used for cyclic Tx tests were reconstituted by air pluviation of the dry sand and the fabric stability that a sand may acquire in situ thanks to the processes of natural deposition, ageing, stress and strain history, overconsolidation and cementation were not reproduced. As a consequence, the experimental cyclic resistance curves should be considered as lower bounds for the tested sands. Same concepts can be applied to CPTs.

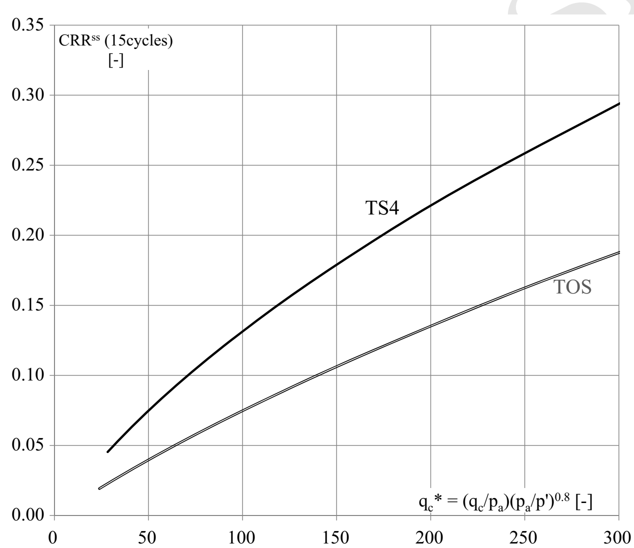

Fig. 13 Relationships between normalised cone resistance q_c^* and cyclic resistance ratio at 15 cycles for unidirectional simple shear conditions CRR_{15}^{SS}. The curves refer to clean, normally consolidated, unaged and uncemented Ticino and Toyoura sands

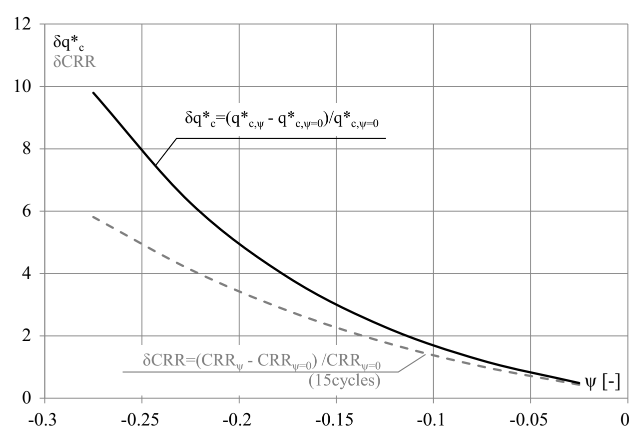

Fig. 14 Increment of q_c^* and CRR respect to their values at $\psi = 0$, caused by a state parameter variations

Journal : Large 11440 Dispatch : 29-10-2015 Pages : 16
Article No. : 419 □ LE □ TYPESET
MS Code : AGEO-D-15-00067 ✔ CP ✔ DISK

- the cyclic Tx tests ~~reproduces~~ reproduced unidirectional loading condition, while, for level ground conditions, earthquake loading is best approximated as two-directional loading, so the CRR from a unidirectional test should be reduced to represent in situ conditions [16].
- no fine content effects were accounted.

The aim of the proposed correlations is to provide a useful instrument to improve the actual knowledge on liquefaction and to give a contribution based on the critical state soil mechanics framework to the development of refined correlations between the cyclic resistance of a sand and the results of cone penetration tests.

5 Closing remarks

The evaluation of the undrained cyclic resistance of sandy deposits is required to forecast the soil behaviour during earthquakes (liquefaction, cyclic mobility); due to the difficulties in obtaining undisturbed samples of most liquefiable soils, the cyclic resistance is usually deduced from field test results like CPTs.

The undrained cyclic resistance and the tip resistance of a cone penetration test of uncemented and unaged sands depend on the soil mineralogy, shape, asperities and roughness of grains, grading and fabric (i.e. material properties), on its aggregation state (density), on the level of the overburden effective stress (confinement or depth). The latter two quantities govern the volumetric behaviour of the soil when sheared and in consequence the two resistances (cyclic and tip). For a given soil the cyclic resistance and the tip resistance can be normalised to the confining stress level, becoming CRR = cyclic resistance ratio at a reference number of cycles, N and $q_c^* = (q_c/p_a) \cdot (p_a/p')^{\beta}$, respectively, so their magnitude depends mainly on the stress change caused by the volumetric strains. The volumetric strains, in turns, can be represented by the state parameter ψ, which indicates the potential dilation or contraction behaviour of the soil during shearing.

The evaluation of undrained cyclic resistance of Ticino and Toyoura sands was achieved through undrained cyclic tests on reconstituted specimens. A relationship between CRR, ψ and N was defined for both sands. The cyclic resistance of TS4 is higher than that of TOS at the same value of the state parameter ψ. TS4 has a higher critical stress ratio M_c than TOS since the grains of TS4 are more irregular and angular than those of TOS, so the frictional work is greater in TS4 than TOS: in cyclic loading more energy is dissipated and the resistance grows. Moreover, TS4 is more compressible than TOS: higher compressibility may imply that a larger part of the undrained cyclic load applied during tests on TS4 samples is spent to compress and rearrange the sand grains than in TOS.

The tip resistance was deduced from CPTs performed in centrifuge with a miniaturised piezocone on homogeneous reconstituted models of TS4 and TOS. The test interpretation allowed the quantification of the effects of two major parameters on the resistance: the first given by the overburden stresses acting at the depth of the tip, the second, and more relevant at depths commonly investigated via CPTs (<50 m), is due to the increment of stresses around the tip caused by the penetration. A relationship between the normalised cone resistance q_c^* and ψ was calibrated for both sands. The higher values of q_c^* from tests on dense TOS ($\psi < -0.15$) respect to those inferred from tests performed on dense TS4 could be due to the lower crushability of quartz TOS respect to feldspathic TS4.

The proposed method for evaluating the cyclic resistance of a young, clean sand, uncemented and normally consolidated, from the results of cone penetration tests is based on the state parameter assumed as independent variable of both normalised resistances, CRR and q_c^* (Eq. 13). A correlation usable in the engineering practice will require a calibration on a wider number of sands to account for the effects of mineralogy, shape, asperities and roughness of grains and grading. Also different deposition methods of the reconstituted samples need to be considered since grain contact arrangement is a key factor in cyclic resistance of sand. Finally a validation on sites where liquefaction occurred is desirable.

Acknowledgments The authors gratefully acknowledge the ISMGEO (Istituto Sperimentale Modelli Geotecnici in Bergamo, Italy) to have provided the triaxial tests results on TS4 and the centrifuge test results on TS4 and TOS.

References

1. Baldi G, Bellotti R, Ghionna V, Jamiolkowski M, Pasqualini E (1982) Design parameters for sand from CPT. In: Proceedings of ESOPT 2. Amsterdam
2. Baldi G, Bellotti R, Ghionna N, Jamiolkowski M, Pasqualini E (1986) Interpretation of CPTs and CPTU's, 2nd Part. In: Proceedings of the 4th international geotechnical seminar, Nanyang Technological Institute. Singapore, pp 143–156
3. Baldi G, Belloni G, Maggioni W (1988) The ISMES geotechnical centrifuge. In: Corté JF (ed) Centrifuge 88, Paris. Balkema, Rotterdam, pp 45–48
4. Been K, Jefferies MG (1985) A state parameter for sands. Géotechnique 35(2):99–112
5. Been K, Crooks JHA, Becker DE, Jefferies MG (1986) The cone penetration test in sands: part I, state parameter interpretation. Géotechnique 36(2):239–249
6. Bellotti R, Crippa V, Pedroni S, Ghionna VN (1988) Saturation of sand specimen for calibration chamber tests. In: Proceedings of ISOPT-1, Orlando, Vol. 2. pp 661–672
7. Bolton MD, Gui MW, Garnier J, Corte JF, Bagge G, Laue J, Renzi R (1999) Centrifuge cone penetration tests in sand. Geotechnique 49(4):543–552

Journal : Large 11440 | Dispatch : 29-10-2015 | Pages : 16
Article No. : 419 | LE | TYPESET
MS Code : AGEO-D-15-00067 | CP | DISK

8. Boulanger RW, Idriss IM (2004) State normalization of penetration resistance and the effect of overburden stress on liquefaction resistance. In: Proceedings of the 11th international conference on soil dynamics and earthquake engineering, Berkeley. American Society of Civil Engineers. Reston, 7–9 Jan 2004, pp 484–491
9. Carter JP, Yeung SK (1985) Analysis of cylindrical cavity expansion in a strain weakening material. Comput Geotech 1:161–180
10. Carter JP, Booker JR, Yeung SK (1986) Cavity expansion in cohesive frictional soils. Géotechnique 36(3):349–358
11. Cetin KO, Isik NS (2007) Probabilistic assessment of stress normalization for CPT data. J Geotech Geoenviron Eng ASCE 133(7):887–897
12. Fioravante V, Jamiolkowski M, Tanizawa F, Tatsuoka F (1991) Calibration chamber tests on Toyoura sand. In: Proceeding of the 1st international symposium on calibration chamber testing ISOCCT1 Potsdam. New York, pp 135–146
13. Ghionna N, Porcino D (2006) Evolution of sand microstructure during shear. J Geotech Geoenviron Eng ASCE 132(2):194–202
14. Idriss IM, Boulanger RW (2004) Semi-empirical procedures for evaluating liquefaction potential during earthquakes. In: Doolin D et al. (eds) Proceedings 11th international conference on soil dynamics and earthquake engineering and 3rd international conference on earthquake geotechnical engineering, Stallion Press, Vol 1. pp 32–56
15. Idriss IM, Boulanger RW (2008) Soil liquefaction during earthquakes. Earthquake Engineering Research Institute. MNO-12. Oakland, CA
16. Ishihara K (1996) Soil behavior in earthquake geotechnics, 46th edn. In: The Oxford Engineering Science. Oxford University Press, New York
17. Ishihara K, Iwamoto S, Yasuda S, Takatsu H (1977) Liquefaction of anisotropically consolidated sand. In: Proceedings 9th international conference on soil mechanics and foundation engineering, Japanese Society of Soil Mechanics and Foundation Engineering, Vol. 2. Tokyo, pp 261–64
18. Ishihara K, Yamazaki A, Haga K (1985) Liquefaction of K_0 consolidated sand under cyclic rotation of principal stress direction with lateral constrain, soils and foundations. Jpn Soc Soil Mech Found Eng 5(4):63–74
19. Jaky J (1944) The coefficient of earth pressure at rest. J Soc Hung Archit Eng (Budapest), 355–358
20. Jamiolkowski MB, Lancellotta R, Lo Presti DCF, Pallara O (1994) stiffness of Toyoura sand at small and intermediate strain. In: Proceedings of the 13th international conference on soil mechanics and foundation engineering. New Dheli, pp 169–162
21. Jamiolkowski MB, Lo Presti DCF, Manassero M (2003) Evaluation of relative density and shear strength from CPT and DMT. Soil behavior and soft ground construction, ladd symposium, MIT, Cambridge Mass. Geotechnical Special Publication No. 119, ASCE, Reston, Virginia, pp 201–238
22. Jefferies M, Been K (2006) Soil liquefaction. A critical state approach. Taylor and Francis, London
23. Ladd RS (1977) Specimen preparation and cyclic stability of sands. J Geotech Eng Div ASCE 103:535–547
24. Li X-S, Wang Z-L (1998) Linear representation of steady state line for sand. J Geotech Geoenviron Eng ASCE 124(12): 1215–1217
25. Li XS, Dafalias YF (2000) Dilatancy for cohesionless soils. Géotechnique 50(4):449–460
26. Moss RES, Seed RB, Kayen RE, Stewart JP, Der Kiureghian A, Cetin KO (2006) CPT-based probabilistic and deterministic assessment of in situ seismic soil liquefaction potential. J Geotech Geoenviron Eng ASCE 132(8):1032–1051
27. Mulilis JP, Seed HB, Chan CK, Mitchell JK, Arulanandan K (1977) Effect of sample preparation on sand liquefaction. J Geotechnical Eng Div ASCE 103(GT2):91–108
28. Olsen RS, Malone PG (1988) Soil classification and site characterization using the cone penetrometer test. In: Penetration Testing 1988, ISOPT 1, De Ruiter, Vol. 2. Balkema, Rotterdam, pp 887–893
29. Robertson PK, Campanella RG (1985) Liquefaction potential of sands using the cone penetration test. J Geotech Eng ASCE 22(3):298–307
30. Robertson PK, Wride CE (1998) Evaluating cyclic liquefaction potential using the cone penetration test. Can Geotech J 35(3):442–459
31. Robertson PK (1999) Estimation of minimum undrained shear strength for flow liquefaction using the CPT. In: Proceedings of the 2nd international conference on earthquake geotechnical engineering. Balkema, Rotterdam.
32. Robertson P (2010) Evaluation of flow liquefaction and liquefied strength using the cone penetration test. J Geotech Geoenviron Eng 136(6):842–853
33. Rowe PW (1962) The stress dilatancy relation for static equilibrium of an assembly of particles in contact. Proc R Soc Lond A 269:500–527
34. Salgado R, Mitchell J, Jamiolkowski M (1997) Cavity expansion and penetration resistance in sand. J Geotech Geoenviron Eng 123(4):344–354
35. Schmertmann JH (1976) An updated correlation between relative density D_R and fugro-type electric cone bearing, q_c. Contract Report DACW 39-76 M 6646 WES, Vicksburg, Miss.
36. Schmertmann JH (1978) Guidelines for cone penetration test, performance and design, Report FHWA-TS-787-209, Federal Highway Administration, Washington, July 1978
37. Seed HB, Idriss IM (1982) Ground motions and soil liquefaction during earthquakes. Earthquake Engineering Research Institute Monograph, Oakland
38. Toki S, Tatsuoka F, Miura S, Yoshimi Y, Yasuda S, Makihara Y (1986) Cyclic undrained triaxial strength of sand by a cooperative test program. Soils Found 26(3):117–128
39. Verdugo R (1992) The critical state of sands: discussion. Géotechnique 42(4):655–663
40. Verdugo R, Ishihara K (1996) The steady state of sandy soils. Soils Found 36(2):81–91
41. Youd TL, Idriss IM, Andrus RD, Arango I, Castro G, Christian JT, Dobry R, Finn WDL, Harder LF, Hynes ME, Ishihara K, Koester JP, Liao SSC, Marcuson WF, Martin GR, Mitchell JK, Moriwaki Y, Power MS, Robertson PK, Seed RB, Stokoe KH (2001) Liquefaction resistance of soils: summary report from the 1996 NCEER and 1998 NCEER/NSF Workshops on evaluation of liquefaction resistance of soils. J Geotech Geoenviron Eng ASCE 127(10):817–833
42. Zhang G, Robertson PK, Brachman RWI (2002) Estimating liquefaction-induced lateral displacements using the standard penetration test or cone penetration test. J Geotechn Geoenviron Eng ASCE 130(8):861–871

Journal : **Large 11440**	Dispatch : **29-10-2015**	Pages : **16**
Article No. : **419**	☐ LE	☐ TYPESET
MS Code : **AGEO-D-15-00067**	☑ CP	☑ DISK